JOINT INSTITUTE FOR NUCLEAR RESEARCH

Bogoliubov Laboratory of Theoretical Physics (BLTP)

FINAL REPORT ON THE START PROGRAMME

Numerical Simulation of Spintronic Effects in Josephson Nanojunctions

Supervisor:
Dr. Majed Nashaat
BLTP, JINR, Dubna, Russia

Student:
Ossama W. Abdelwahed (3rd year B.Sc Physics)
Alexandria University
Alexandria, Egypt

Participation period:

7 August - 1 October, 2022

Dubna 2022

Abstract

Several interesting phenomena has been observed in the field of spintronics that had an immense impact on the development of information technology. Further progress in this field is based on better understanding of magnetization patterns and how to exploit the association between the electrical and magnetic characteristics of electrons which is our aim in this practice. In the first part, we study the hysteresis loop for several ferromagnetic materials using micromagnetic simulation. The results show a strong dependence of the coercivity on the exchange, anisotropic and Dzyloshinskii-Morayia constants. In the second part, we consider point-contact Josephson junction. We investigate the effect of junction capacitance, and external radiation on the junction IV-curves. Finally, we demonstrate the effect of Rashba and Dresselhaus spin-orbit-coupling (SOC) in superconductor-ferromagnet-superconductor Josephson junction. Results show that the appearance of negative-differential-resistance and locking steps in the IV are enhanced for material with strong Rashba and weak Dresselhaus SOC.

Contents

1 Micromagnetic Simulation **1**

1.1 Introduction 1

1.2 Hysteresis Simulation 1

1.2.1 Results 2

1.3 FMR simulation 4

1.3.1 Results 4

2 Simulation of Josephson Junctions **5**

2.1 Introduction 5

2.2 SIS Junction 6

2.2.1 Model 6

2.2.2 Results 7

2.2.2.1 Effect of External Radiation 8

2.3 SFS Junction 9

2.3.1 Model 9

2.3.2 Results 11

2.3.2.1 Pure Rashba SOC 11

2.3.2.2 Rashba-Dresselhaus SOC 12

3 Conclusion **15**

4 Prospects **16**

5 Acknowledgement **16**

1 Micromagnetic Simulation

1.1 Introduction

Magnetic materials have been the interest of considerable research due to their applications in industry and information technology, most recently in spin valves and magnetoresistive memory [1]. The design and function of many modern devices require the understanding of magnetization patterns on a sub-microscale which is what micromagnetics deal with. Most Magnetic systems can be studied using continuum models where the magnetization $\mathbf{M}(\mathbf{r}, t)$ is considered to be a temporally and spatially continuous differentiable vector field, with a constant norm equal to the saturation magnetization $|\mathbf{M}| = M_s$. We often use the normalized magnetization field $\mathbf{m}(\mathbf{r}, t) = \mathbf{M}(\mathbf{r}, t)/M_s$, constrained by $m_x^2 + m_y^2 + m_z^2 = 1$. Magnetization is then used to define an energy density field which is the sum of several energy terms $w(\mathbf{m}) = \sum_i w_i(\mathbf{m})$. Integrating $w(\mathbf{m})$ over the volume of our system results in the energy functional $E[\mathbf{m}] = \int w(\mathbf{m})dV$ which is minimized to find equilibrium states of our system. The temporal evolution of how magnetization changes to minimize the system's energy is governed by the Linda-Lifshitz-Gilbert (LLG) equation [2].

$$\frac{d\mathbf{M}}{dt} = -\gamma \mathbf{M} \times \mathbf{H}_{eff} + \frac{\alpha}{M_0}\left(\mathbf{M} \times \frac{d\mathbf{M}}{dt}\right) \tag{1}$$

where γ is the gyromagnetic ration, α is the phenomenological Gilbert damping constant, and $\mathbf{H}_{eff} = \frac{1}{\mu_0 M_s}\frac{\delta w(\mathbf{m})}{\delta \mathbf{m}}$ is the effective field computed as the first variational derivative of energy density where μ_0 is the magnetic permittivity of free space.

In this part of the practice we use Ubermag, a micromagnetic simulation environment [3], to study the behavior of magnetic materials by investigating the effect of energy terms on the hysteresis loop and its key points, and the dynamics of magnetization.

1.2 Hysteresis Simulation

A common measurement taken on magnetic materials is the major hysteresis loop between applied external field $\mu_0\mathbf{H}$ and the sample's magnetization $\mathbf{m}$ and the quantities that describe its key points. Here an adaptation of the first standard problem proposed by μMag group is used to investigate the effect of different energy terms on the hysteresis loop. The sample to simulate is a thin film with dimensions measuring $120 \times 120 \times 10nm$, geometry shown in Fig.(1). The material is assumed to have one easy axis of anisotropy along the y axis [4]. The energy terms we consider in our investigation are, the Zeeman energy $w_z = -\mu_0 M_s \mathbf{m} \cdot \mathbf{H}$, uni-axial anisotropy $w_a = -K(\mathbf{m} \cdot \mathbf{u})$, where $\mathbf{u}$ is the easy axis direction, exchange energy

$w_{ex} = A(\nabla \mathbf{m})^2$, and Dzyaloshinskii-Moriya energy $w_d m = D[m_z \nabla \cdot \mathbf{m} - (\mathbf{m} \cdot \nabla) m_z]$ that aligns moments perpendicular to each other, resulting in the following energy functional.

$$E = \int \left[-\mu_0 M_s \mathbf{m} \cdot \mathbf{H} + -K(\mathbf{m} \cdot \mathbf{u}) + A(\nabla \mathbf{m})^2 + D[m_z \nabla \cdot \mathbf{m} - (\mathbf{m} \cdot \nabla) m_z] \right] dV \qquad (2)$$

The initial conditions for our simulation was $M_s = 8.0 \times 10^5 A/m$ in the negative y direction which was arbitrary chosen. The discretization cell dimensions are $5nm \times 5n \times 5nm$ resulting in 1152 cells. Given the energies and field we use Ubermag's hysteresis driver which uses OMMFF's "*Osx_ MinDriver*" that advances the state of our system from the initial configuration by direct energy minimization. In the simulation an external field is applied in the y from $-200mT$ to $200mT$ and back in 400 steps [2, 5].

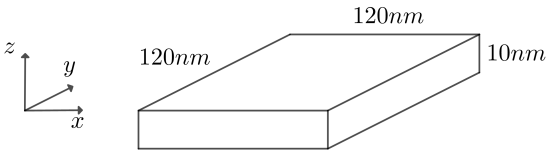

Figure 1: Dimensions of sample used in both simulations.

1.2.1 Results

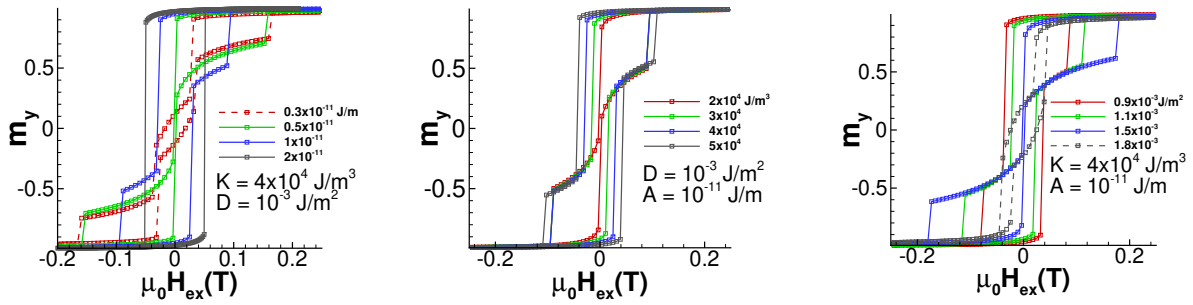

(a) (b) (c)

Figure 2: Results of Ubermag hysteresis simulation, (a) shows hysteresis for different value of A, (b) shows hysteresis for different values of K, and (c) shows hysteresis for different valuues of D.

We can see from Fig.(2a) and Fig.(2b) that both the exchange interaction and the anisotropty energy have a similar effect on the coercivity of our hysteresis, both increasing it. This is expected since the exchange energy tend to align magnetic moments parallel to each other which results in the material withstanding a higher external field before it changes orientation. In

similar fashion the anisotropy energy tend to align moments parallel or anti-parallel to the easy axis which is in our case parallel to the external field. On the other hand, we notice that DMI having the opposite effect since it tends to align moments perpendicular to each other decreasing the coercivity.

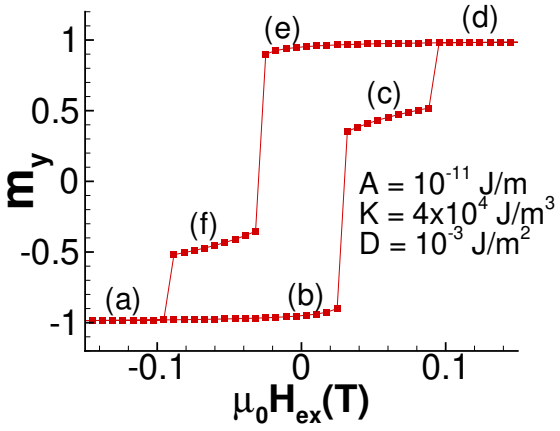

Figure 3: hysteresis loop for the indicated simulation parameters

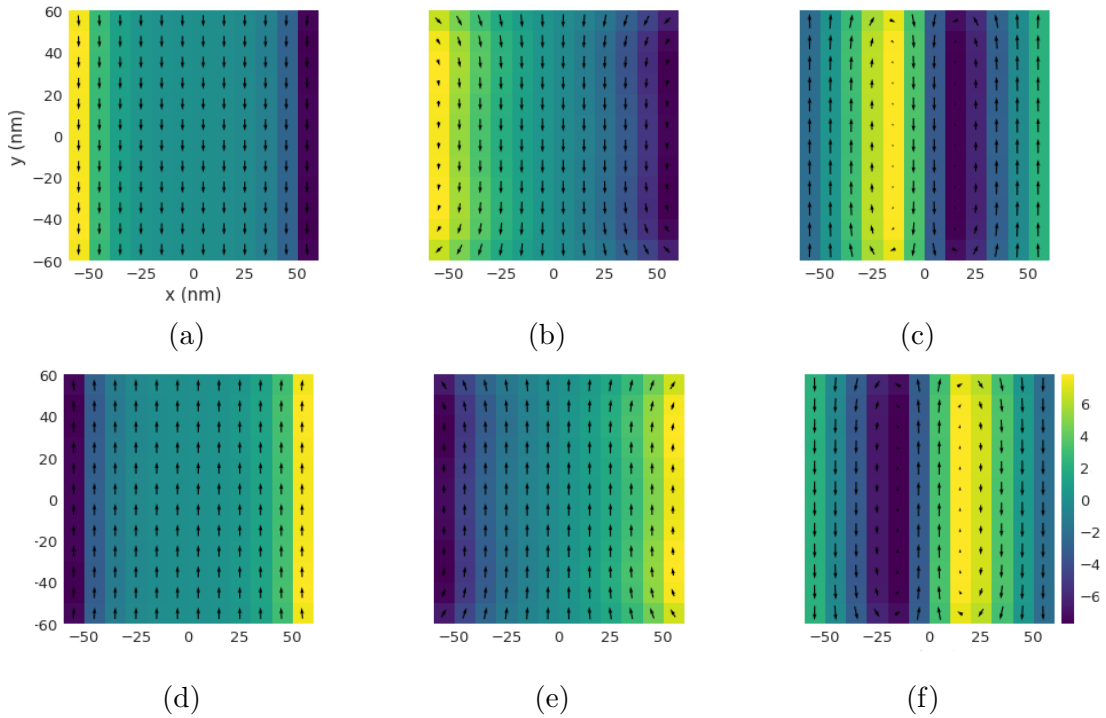

Figure 4: Projection of the xy-plane of the sample simulated at different locations of hysteresis loop in Fig.(3). Arrows represent the x and y components of **m** and color determines the z component.

In Fig.(4a) and Fig.(4d) our sample is in a saturated state, we can see that the magnetization

is almost uni-formally oriented in the direction of the applied field with some canting of magnetization near the edges of the sample, this is the result of the self-magnetostatic field or demagnetization field resulting from the geometry of the sample [4]. As the field is weakened the canting increases as seen in Fig.(4b) and Fig.(4e) till the nucleation field is reached and domain wall pinning occurs where we observe the growth of the reverse domain [6].

1.3 FMR simulation

This simulation is based on the problem proposed in reference [7] aiming to get numerical calculations of the ferromagnetic spectrum and identifying the ferromagnetic resonance (FMR). The same geometry as in Fig.(1) is used. The sample is assumed to be a Permalloy with an easy axis in the z direction and $A = 1.3 \times 10^{-11} J/m$. An external magnetic field with magnitude $H = 80kA/m$ is applied along the direction $(1, 0.715, 0)$. First, we initialize the system with a uniform out-of-plane magnetization $\mathbf{m} = (0, 0, 1)$. The system is allowed to relax for $5ns$ to obtain sn equilibrium magnetization configuration, the final relaxed magnetization configuration is saved to serve as the initial configuration for the next dynamic stage. The energy of the system is minimized by integrating the LLG equation with a large Gilbert damping $\alpha = 1$ for $5ns$. In the next step, a simulation is started using the equilibrium magnetization configuration as the initial configuration. Now, the direction of an external magnetic field is altered to $(1, 0.7, 0)$. This simulation stage runs for $20ns$ while the (average and spatially resolved) magnetization is recorded every $5ps$. The Fourier transform of the time evolution is computed resulting in the ferromagnetic frequency spectrum where FMR can be determined. The Gilbert damping is the dynamic stage is varied to observe its effect.

1.3.1 Results

As the Gilbert damping coefficient increases the perccesion is dissipated in a faster manner and the magnetization reaches its stable point faster. From Fig.(5) we can identify the FMR from the maximal amplitude in the frequency spectrum, we can also notice that at very low Gilbert damping another peak known as the nutation peak which is a result of the inertia of magnetic percession being significant compared to the damping [8, 9] which we can also observe in the time evolution of average magnetization where the amplitude is not uni-formally decaying at $\alpha = 0.008$. We also observe that as the damping decreases, the FMR line-width become very sharp.

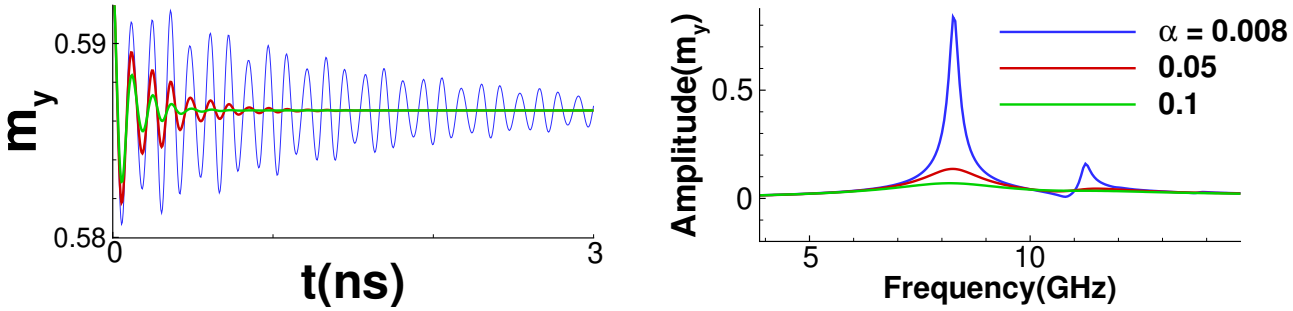

Figure 5: (a) The average y component of magnetization time evolution, (b) The ferromagnetic frequency spectrum resulted from the Fourier transform of (a)

2 Simulation of Josephson Junctions

2.1 Introduction

The Josephson effect was discovered by Brain Josephson in 1962 [10].Josephson predicted that a supercurrent I_s can exsit between two superconductors separated by a thin insulating layer (SIS) and its value is proportional to the sine of the gauge-invariant phase difference $i_s = i_c sin\varphi$ (where i_c is the critical current). Further studies extended the effect beyond Josephson's prediction in that the supercurent can exist if the superconductors and connected by a weak link of any physical nature [11]. Since that time there has been a growing interest in the fundamental physics and applications of that phenomena. The development in Josephson junction technology have made it possible to develop a variety of ultralow magnetic fields sensors, measure universal constants more accurately, as well as the design of integrated circuits for signal processing and general computing [12–14]. A particularly interesting and promising Josephson structure is the superconductor-ferromagnet-superconductor (SFS) junction. The spin-orbit interaction in a ferromagnet lacking inversion symmetry allows for a direct coupling between the magnetic moment and supercurrent. In such junctions where time reversal symmetry is broken the current-phase relation (CPR) is defined as $i_s = i_c sin(\varphi - \varphi_o)$ where the phase shift φ_o is proportional to the magnetic moment perpendicular to the gradient of the asymmetric spin-orbit potential [15]. This allows for the control of magnetic moment percession via Josephson current. Junctions with such phase shift are called φ_0 junctions and they show promising prospects for spintronics and information technology [15, 16].

2.2 SIS Junction

2.2.1 Model

In our investigation, we consider the nonzero voltage state of the junction, thus we have to take into consideration additional current channels relevant in the voltage state. We neglect the spatial variation of the phase difference of the superconductors and only consider temporal variation $\varphi(\tau)$, and the magnetic field generated by the the Josephson current, this can be achieved by assuming that spatial dimensions of the junction's area are smaller than the Josephson penetration depth λ_j [17], thus the current associated with the weak coupling is given by $i_s = i_c sin(\varphi(\tau))$ where i_c is the critical current. In situations where not only the voltage but also its time derivative is nonzero we must include the displacement current $i_d = C\frac{dv}{d\tau}$determined by the characteristic capacitance of the junction C. And normal current $i_N = \frac{v}{R}$ due to quasiparticle tunneling and resistivity flux flow, approximated by an Ohmic resistance. We then arrive to the resistivity and capacitively shunted junction model (RCSJ) [17–19].

The net current through the junction is given according to Kirchhoff's law as

$$i_{net} = i_c sin\varphi + \frac{v}{R} + C\frac{dv}{d\tau} \tag{3}$$

togther with Josephson's voltage-phase relation

$$\frac{d\varphi}{d\tau} = \frac{2e}{\hbar}v \tag{4}$$

forms the basic equation governing our system. the two equations can be normalized. We normalize the current by the critical current $I = i_{net}/i_c$, time and voltage with plasma frequency $t = \omega_p\tau$, $V = 2ev/\hbar\omega_p$, where $\omega_p = \sqrt{2ei_c/C\hbar}$, and $\beta = \frac{1}{R}\sqrt{\hbar/2ei_cC} = 1/\sqrt{\beta_c}$ is the reciprocal square root of the McCumber parameter, obtaining

$$\begin{cases} \frac{dV}{dt} = I - sin\varphi - \beta V \\ \frac{d\varphi}{dt} = V \end{cases}$$

in the case of external radiation, we consider it as Ac- current source [17], and our new equations become

$$\begin{cases} \frac{dV}{dt} = I - sin\varphi - \beta V + Asin\omega t \\ \frac{d\varphi}{dt} = V \end{cases}$$

where A is the amplitude of the external radiation, and ω is its angular frequency. The system of equation is solved using fourth order Runge-Kutta method. Sample C++ code was

provided by the BLTP group and another was developed by me using python and the results are compared.

2.2.2 Results

We notice clear distinction between current-voltage characteristics (IVC) shown in Fig.(6) for underdamped ($\beta < 1$) where the junction capacitance and/or resistance are large and overdamped ($\beta > 1$) where capacitance and/or resistance are small. Whereas for overdamped junction the same IVC is observed for increasing or decreasing current, for underdamped junction when decreasing the current the junction stays in the nonzero voltage state even below I_c, while increasing the current from zero the underdamped junction stays in the zero voltage state till it reaches the critical current I_c which results in the appearance of a hysteretic IVC for the underdamped junction.

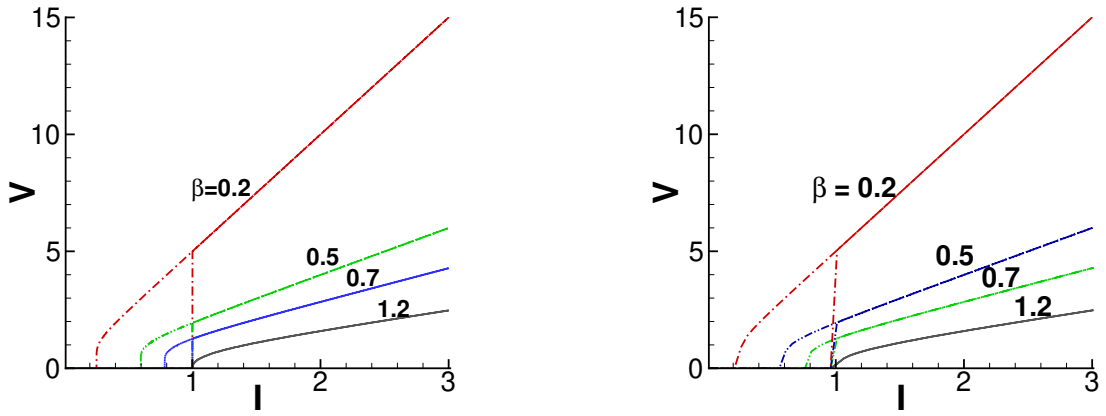

(a) C++ (b) Python

Figure 6: Current-voltage characteristic curve for different values of β. A hysteresis appear for underdamped junction ($\beta < 1$) where the return current is effected by the value of β.

We see from IVC that for $I > I_c$ part of the current is flowing as normal or displacement current at finite average junction voltage. The finite junction voltage results in a temporal variation in Josephson current and, since the total current is fixed, a temporal variation of the sum of the normal and displacement current resulting in a time dependent voltage $V(t)$ which is observed in Fig.(7) [17]. In the overdamped junction we can observe a non-sinusoidal oscillating voltage with long period at $I \approx I_c$, this corresponds to a low time averaged voltage. In the case of $I >> I_c$ we observe that the period of the voltage oscillation decreases resulting in an almost sinusoidal voltage and a higher time averaged voltage.

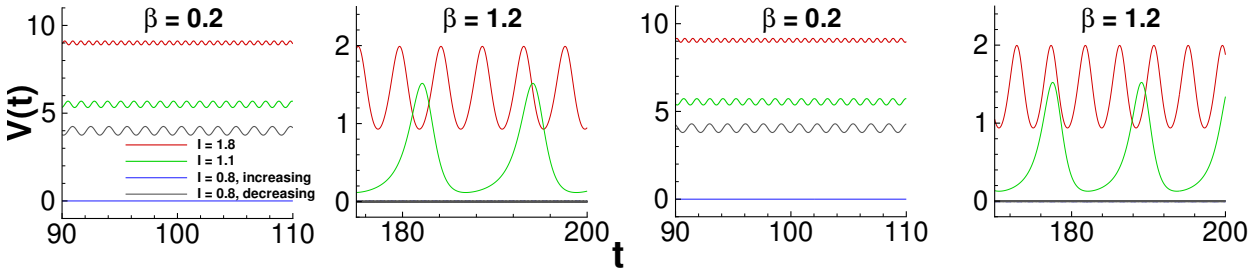

(a) C++ (b) C++ (c) Python (d) Python

Figure 7: Time dependence of the voltage for under and overdamped junction

2.2.2.1 Effect of External Radiation

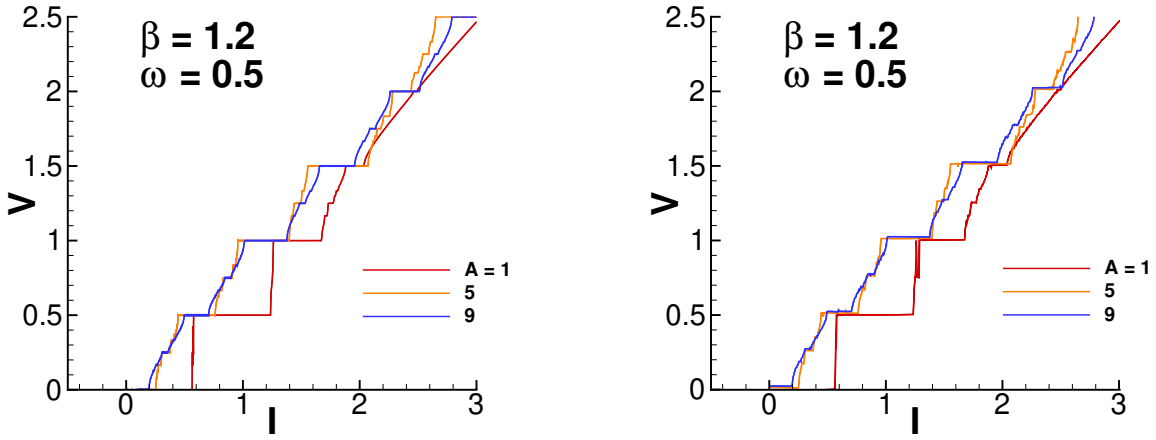

(a) C++ (b) Python

Figure 8: The appearance of supercurrent steps in the IVC at integer multiples of the radiation frequency, which is known as Shapiro steps.

The appearance of current steps at fixed voltages is due to the synchronization of the phase change with the external radiaition source, this occures not only at voltages that match the frequency of external radiaiton but also at higher harmonics of the signals frequency due to the nonlinearity of the juction [17], The n*th* step corresponds to the phase locking of the junction's oscillation by the n*th* harmonic.

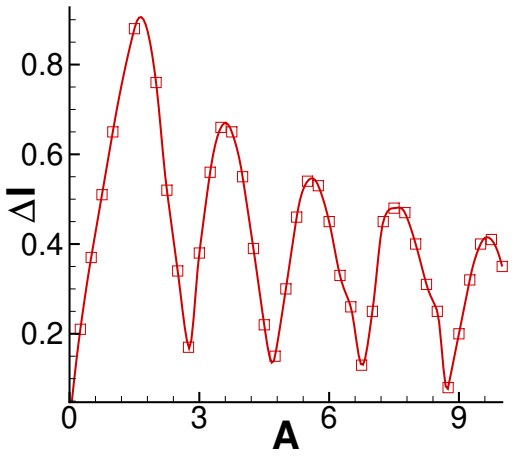

Figure 9: The width of the first Shapiro step $n = 0$ plotted as a function of the amplitude of external radiation

In the presence of external radiation in an overdamped junction, the Josephson current is expressed as a Fourier-Bessel series. And for the nth harmonic the width of first Shapiro step is given in [17] as

$$\Delta I = I_c \left| J_n \left(\frac{2\pi A}{\Phi_0 \omega} \right) \right| \tag{5}$$

where J_n is the nth order Bessel function of first kind. This relation is demonstrated in our calculations in the effect of external radiations amplitude on the width of the first Shapiro step in Fig.(9), which has a Bessel function dependence.

2.3 SFS Junction

2.3.1 Model

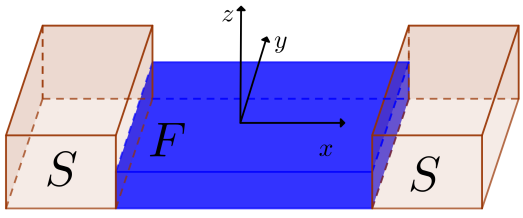

Figure 10: Geometry of the considered SFS φ_0 junction. The ferromagnetic film has an easy axis directed along the z-axis and the Josephson current flows in the x diction.

We consider an SFS anomalous Josephson junction with SOC [16], the geometry is shown in Fig.(10), where the F layer is a thin film with an easy-axis magnetic anisotropy directed along

the z-axis. Both the easy-axis and the gradient of the asymmetric spin-orbit potential are along the z-axis. Due to the interplay between the exchange field and the SOC, the CPR of the SFS junction is given as $I = I_c sin(\varphi - \varphi_0)$, The anomalous phase shift ϕ_0 is dependent on SOC and the geometry of the device. Taking into consideration a two dimensional SOC with momenta in the x-y plane with both Rashba and Dresselhaus contribution, the anomalous phase shift for the particular geometry considered according to [20] can be written in the following form:

$$\varphi_0 = r_{\tilde{\beta}}(\tilde{\beta} m_x + m_y) \tag{6}$$

where $\tilde{\beta} = \beta/\delta$ is the ratio between SOC coefficients, where β is the Dresselhaus coefficient, δ is the Rashba coefficient, $r_{\tilde{\beta}} = r(1 - \tilde{\beta})$ is the SOC strength accounting for the dependence of both δ and β.

The dynamics of magnetization of the F lyer is described by the Landau-Lifshitz-Gilbert (LLG) Eq.(1). Here taking into account the expression 6 for the phase shift, the effective field according to [20] is given as:

$$\mathbf{H}_{eff} = \frac{K}{M_0}[G r_{\tilde{\beta}} sin(\varphi - \varphi_0)(\tilde{\beta}\hat{\mathbf{x}} + \hat{\mathbf{y}}) + m_z \hat{\mathbf{z}}] \tag{7}$$

where $G = E_J/(K\nu)$ is the ratio of the Josephson energy to the magnetic one where K is the anisotropic energy term, ν is the volume of the ferromagnetic layer.

$$\begin{aligned}
\dot{m}_x &= \frac{\omega_F}{1 + M_s\alpha^2}\left\{m_z[h_y + \alpha(h_x m_z - h_z m_x)] + h_x \alpha m_y^2 - m_y(h_z + h_y \alpha m_x)\right\} \\
\dot{m}_y &= \frac{\omega_F}{1 + M_s\alpha^2}\left\{m_x[h_z + \alpha(h_y m_x - h_x m_y)] + h_y \alpha m_z^2 - m_z(h_x + h_z \alpha m_y)\right\} \\
\dot{m}_z &= \frac{\omega_F}{1 + M_s\alpha^2}\left\{m_y[h_x + \alpha(h_z m_y - h_y m_z)] + h_z \alpha m_x^2 - m_x(h_y + h_x \alpha m_z)\right\} \\
\dot{V} &= \frac{1}{\beta_c}\left[I + A sin(\omega_R t) - sin(\varphi - \varphi_0) - V + r_{\tilde{\beta}}(\tilde{\beta}\dot{m}_x + \dot{m}_y)\right], \qquad \dot{\varphi} = V
\end{aligned} \tag{8}$$

where β_c is the McCumber parameter, $m_i = M_i/M_0$ for $i = x, y, z$ is the normalized magnetization, $m_i = M_i/M_0$ for $i = x, y, z$ is the effective field normalized to K/M_s, $\omega_F = \Omega_F/\omega_c$ here the ferromagnetic resonance frequency $\Omega_f = \gamma K/M_0$ and the characteristic junction frequency $\omega_c = 2eRI_c/\hbar$ and we normalize time in unites of ω_c^{-1}, current in units of I_c, and the voltage in unites of $I_c R$.

From the definition of $\tilde{\beta}$ and the parameter $r_{\tilde{\beta}}$, we can disregard the Dresselhaus contribution by considering $\tilde{\beta} = 0$ thus $r_{\tilde{\beta}} \to r$ and only Rashba SOC is considered. Another possibility is to

have similar contribution of the Rashba and Dresselhaus SOC thus $\tilde{\beta} = 1$, leading to $r_{\tilde{\beta}} = o$ and from expression 6 we see that this will result in the phase-shift vanishing thus decoupling the supercurrrent and magnetic moment and we return to a model similar to that of the SIS junction. This is intriguing since the Rashba SOC can be controlled by a gate voltage giving the possibility of tuning $\tilde{\beta}$, and hence the phase-shift and the supecurrent [21].

This system is solved numerically using the fourth order Runge-Kutta method. First we explore the case of pure Rashba SOC where we explore the manifestation of FMR and the appearance of negative differential resistance (NDR) in the IVC and magnetization locking caused by external radiation. the code used in this part is made by me with python and compared to results of the code provided by my supervisor and BLTP group. The second part we explore both the Rashba and Dresselhaus contribution. In addition to presenting the effects of the Dresselhaus SOC on the IVC we investigate the magnetization dynamics of the system.

2.3.2 Results

2.3.2.1 Pure Rashba SOC

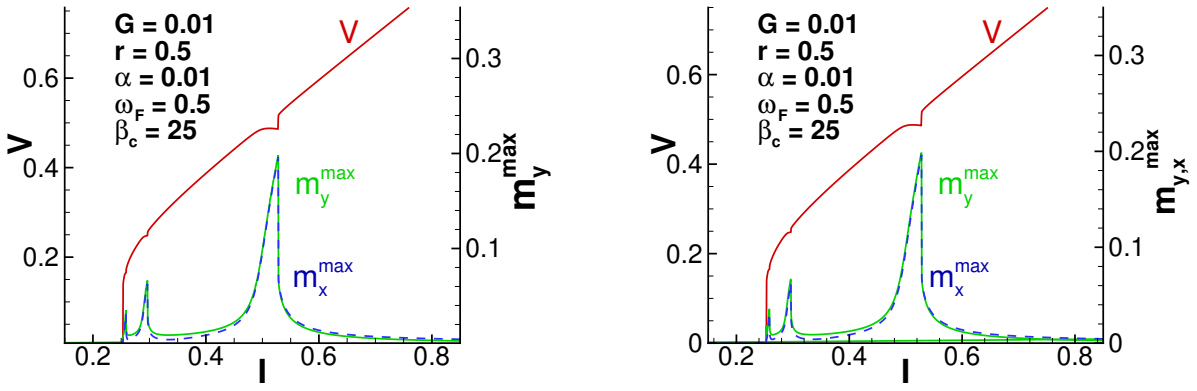

(a) C++ (b) Python

Figure 11: (a) IV characteristics at dieffrent values of Rashba SOC. (b) IV characterstics along with $m_{y,x}^{max}$ in the precense of external radiation

A clear manfistation of the FMR in φ_0 junction can be observed in Fig.(11), where an increase in the magnetization amplitudes m_y^{max} and m_x^{max} near $\omega_F = 0.5$ appear. This signifies that superconducting current provokes the rotation of M to have its components in the xy-plane [22]. This manifestation is also demonstrated in the IVC.

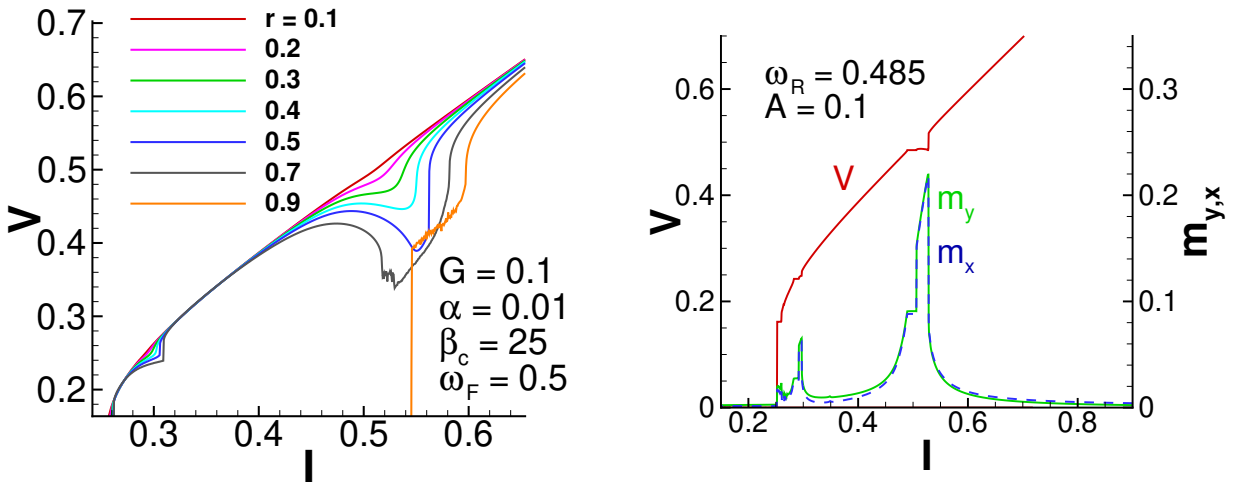

(a) (b)

Figure 12: Manifestation of the FMR in the current dependence of $m_{y,x}^{max}$ and the IVC of the φ_0 junction.

An increae in SOC strength r leads to the manifestation of non-linearity in the IVC and has a notable effect on the IVC in the resonance regeon as shown in Fig.(12a), where the IVC deviates from its linear behavior and a resonance branch appears, a state which clearly demonstrates NDR [23], another notacable thing is the sudden decrease in return current for very high SOC parameter.

The result of applying external radiation on our junction in 11 in the FMR region is presented in Fig.(12b), in addition to the appearance of a shapiro step in the IVC, we observe the appearance of Shapiro like step in x and y components of magnetization, indicating the locking of magnetization percession in the FMR region [23].

2.3.2.2 Rashba-Dresselhaus SOC

In this section, we investigate the effect of Rashba-Dresselhaus SOC ratio on the IV curves. In this case the component of the magnetization in x-direction enter the current phase relation. The IV curves show a region of NDR for $r > 0.3$. In addition to this, we see an increase in the maximum values of the magnetization in x and y components as shown in Fig.(13).

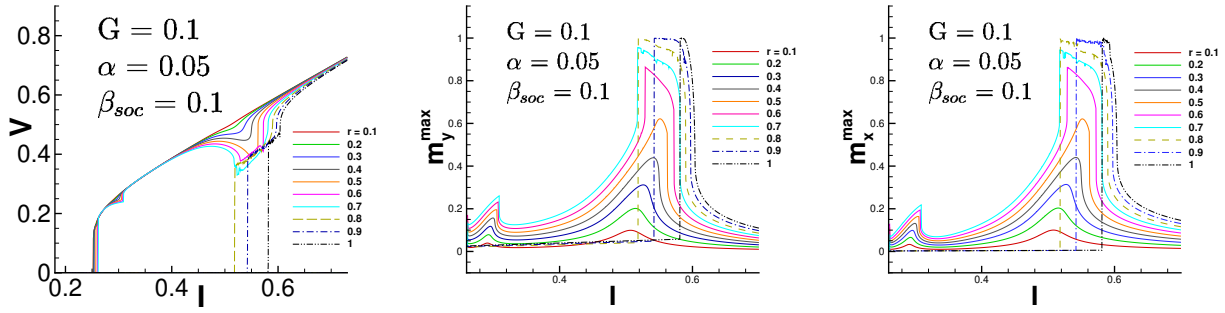

(a) (b) (c)

Figure 13: (a) IV curve at different values of Rashba SOC, in the pressance of Dresselhaus SOC. (b,c) show the corresponding $m_{y,x}^{max}$ current dependence.

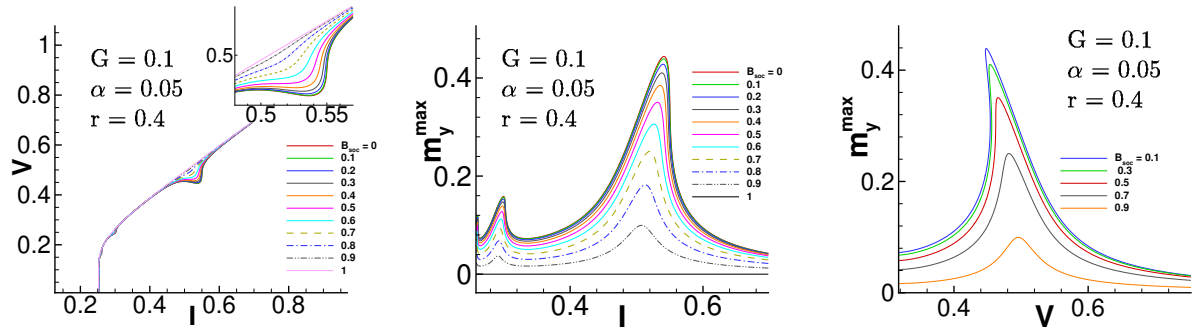

(a) (b) (c)

Figure 14: (a) IV curve at different values of Rashba-Dresselhaus SOC ratio. (b,c) show the corresponding m_y^{max} current and voltage dependence.

In the presence of Dresselhaus SOC, the results show that for strong Dresselhaus SOC strength, the NDR region disappear along with the locking step in m_y^{max} as shown in Fig.(14a) and Fig.(14b). This indicate that $\tilde{\beta}$ has an opposite effect in comparison with r on both the IVC and the magnetization of the system. We also notice that in Fig.(14c) the appearance of the fold-over effect winch is a feature of the Duffing oscillator [24] demonstrating the non-linearity of our system.

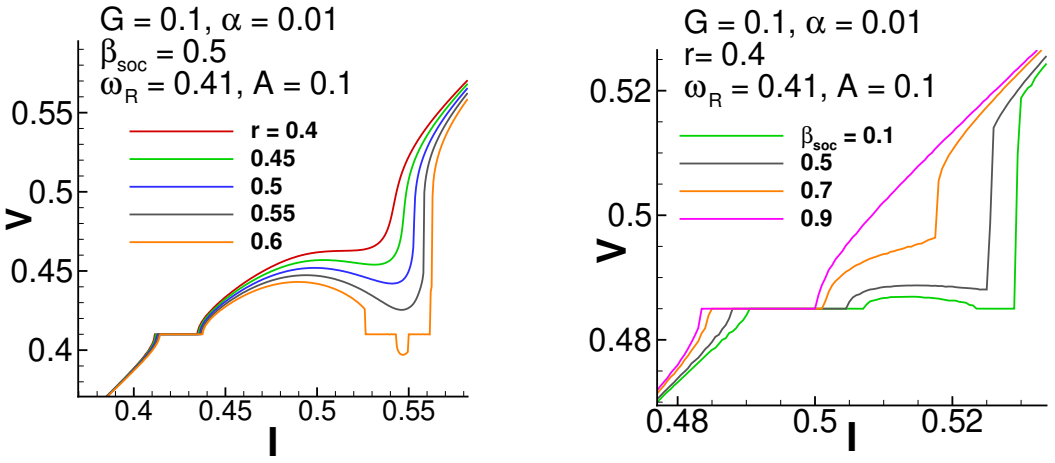

(a) (b)

Figure 15: The IVC under external radiation, (a) shows the effect of the SOC strength and (b) shows the effect of the ratio $\tilde{\beta}$

The effect of external radiation on the IVC at different values of the SOC is demonstrated in figure 15 for fixed radiation frequency and amplitude. We notice the appearance of a hump in the Shapiro step as a manifestation of the FMR and the NDR state [23].

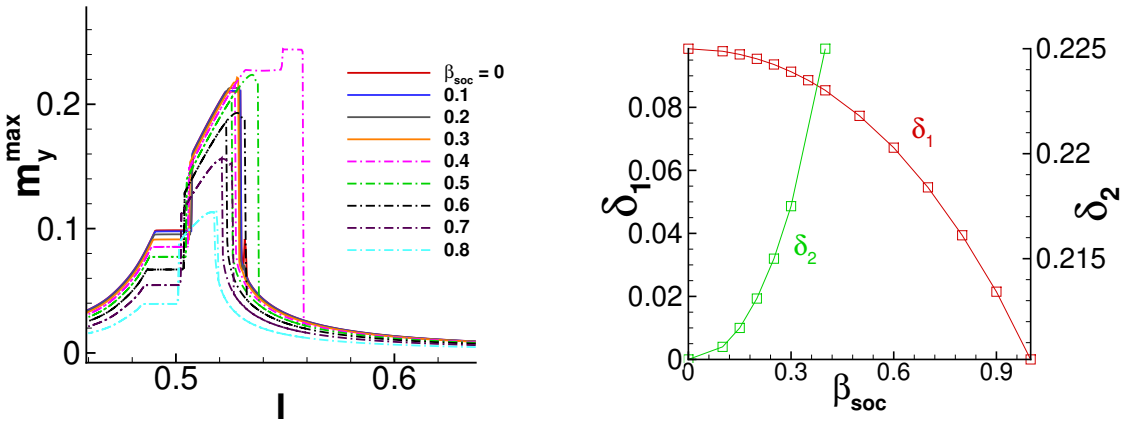

(a) (b)

Figure 16: Effect of the ratio $\tilde{\beta}$ on the hight of magnetization step, (a) shows the current dependence of m_y^{max} and (b) shows the height of the first and second locking steps

In Fig.(16) we show that by increasing in the Dresselhaus SOC relative to Rashba SOC (i.e. the increase in the ratio $\tilde{\beta}$), the first magnetization locking step is shifted downwards and the second locking step in shifted upwards, which is opposite to the effect of SOC strength r as shown in results of [23] in Fig.(3a), assuming pure Rashba SOC. This suggests that the Dresselhause SOC has an opposite effect of that of Rashba SOC.

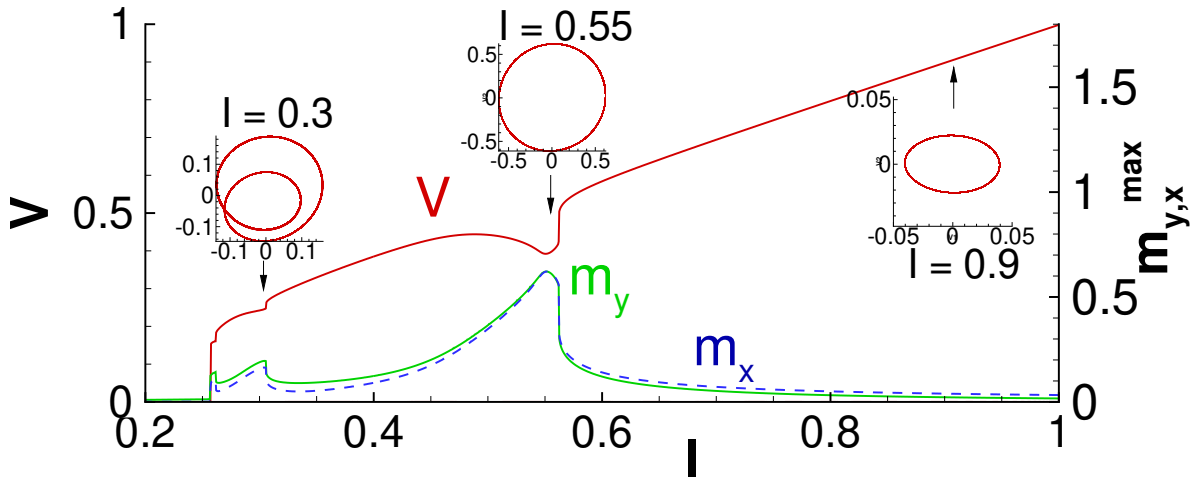

Figure 17: The dynamics of magnetization, sub graphs showing magnetic trajectory of m_y and m_x at different bias currents with no external radiation. Simulation parameters are, $r = 0.5$, $\tilde{\beta} = 0.1$, $G = 0.1$, and $\alpha = 0.01$

In Fig.(18) we demonstrate the magnetization phase trajectories at certain bias current. Trajectories can be characterized by specific shapes. The effect of both the Rashba SOC, represented in the r dependence in (a) and (b), and the Dresselhaus, represented in the $\tilde{\beta}$ dependence in (c) and (d), is shown In figure 18, we can see that they have opposing effects on the magnetization trajectories.

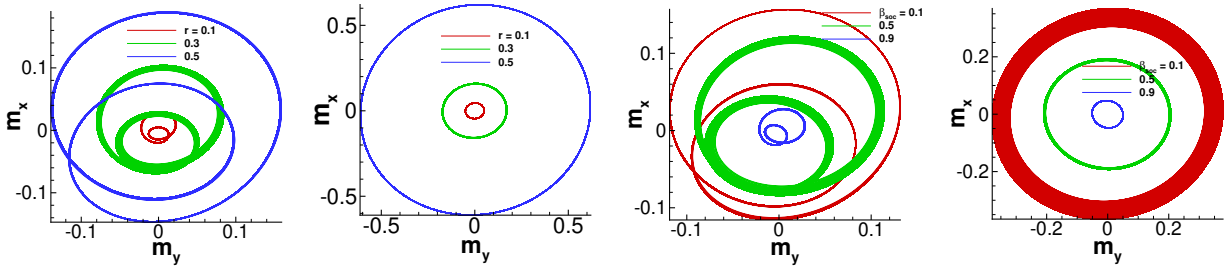

(a) I = 0.3 (b) I = 0.55 (c) I = 0.3 (d) I = 0.55

Figure 18: The figures (a) and (b) show the Effect of changing strength of the SOC r on the magnetic trajectory in the xy-plane and figures (c) and (d) show the effect of changing $\tilde{\beta}$. Simulation parameters are, $r = 0.5$, $G = 0.1$, and $\alpha = 0.01$

3 Conclusion

In this report we study the magnetic hysteresis loop for ferromagnetic material using micro-magnetic simulations. The results show a strong dependence of the coercivity on the exchange, anisotropic and Dzyloshinskii-Morayia constants. The results show that, by increasing the

anistropic constant, the coercivity increased, while the reverse occur for the Dzyloshinskii-Morayia constants. Also, we show that ferromagnetic resonance line width is very sharp for small Gilbert damping values. In the second part, we consider point-contact Josephson junction with insulator barrier. The phase dynamics of the junction demonstrate hysteresis area in the underdamped case. While for junction with zero-capacitance, the hysteresis disappears. In addition to this, external radiation leads to the appearance of Dc-current step "Shapiro steps" in the IV-curves, the width of those steps are strongly depend on the amplitude of the external radiation. Finally, we consider another type of Josephson junction with ferromagnetic layer in the presence of spin-orbit coupling (SOC). In this case, the current phase relation demonstrate a phase shift which depends on the strength of the SOC and dynamics of the magnetization in ferromagnet. The effect of Rashba and Dresselhaus spin-orbit-coupling are investigated in details. The results show that the appearance of negative-differential-resistance and locking steps in the IV are enhanced for material with strong Rashba and weak Dresselhaus SOC.

4 Prospects

A more detailed analysis of the manipulation of magnetization trajectory of the F layer in the SFS φ_0 Josephson junction and the proposal of the possibility of using such Josephson junctions as qubits for quantum computation represent an interesting topic for my upcoming BSc. graduation dissertation.

5 Acknowledgement

I am very grateful to JINR for providing this opportunity and Prof. Dmitri Kazakov the dirctor of BLTP for accepting my application. I would like to give my very great appreciation to my supervisor Dr. Majed Nashaat for his willingness to give his time so generously, encouragement, useful critiques, and his patience with me during the period of my stay both on an academic and personal level. I thank Prof. Yu. Shukrinov and the rest of the condensed matter group in BLTP, Dr. I. Rakhmonov, Dr. K. Kulikov, and A. Mazanik, for their pleasant hospitality and allowing me to join their group discussions. And finally all appreciation for the START organizing team especially Ms. Julia Polyakova and Ms. Elena Karpova for their assistance in organizing my visit.

References

[1] J. Moutinho. Micromagnetic device simulation. Master's thesis, Tcnico Lisboa, April 2017.

[2] M. Beg, R. A. Pepper, and H. Fangohr. Micromagnetics with ubermag. Spintalks and IEEE Magnetic Society, 2020.

[3] M. Beg, M. Lang, and H. Fangohr. Ubermag: Towards more effective micromagnetic workflows. *IEEE Transactions on Magnetics*, 58(2):1–5, 2022.

[4] D. Porter and M. Donahue. Standard problems in micromagnetics. In *Compendium on Electromagnetic Analysis: From Electrostatics to Photonics: Fundamentals and Applications for Physicists and Engineers Volume 1 Electrostatic and Magnetic Phenomena*, pages 285–324. World Scientific, 2020.

[5] D. Porter M. Donahue. Oommf user's guide, release 2.0a3. 2021.

[6] R. Skomski. *Simple models of magnetism*. Oxford University Press on Demand, 2008.

[7] A. Baker, M. Beg, et al. Proposal of a micromagnetic standard problem for ferromagnetic resonance simulations. *Journal of Magnetism and Magnetic Materials*, 421:428–439, 2017.

[8] E. Olive, Y. Lansac, M. Meyer, M. Hayoun, and J-E. Wegrowe. Deviation from the landau-lifshitz-gilbert equation in the inertial regime of the magnetization. *Journal of Applied Physics*, 117(21):213904, 2015.

[9] M. Cherkasskii, M. Farle, and A. Semisalova. Nutation resonance in ferromagnets. *Physical Review B*, 102(18):184432, 2020.

[10] B. D. Josephson. Possible new effects in superconductive tunnelling. *Physics letters*, 1(7):251–253, 1962.

[11] K. K. Likharev. Superconducting weak links. *Reviews of Modern Physics*, 51(1):101, 1979.

[12] R. P. Giffard, J. C. Gallop, and B. W. Petley. Applications of the josephson effects. *Progress in Quantum Electronics*, 4:301–402, 1976.

[13] B. W. Petley. The josephson effects. *Contemporary physics*, 50(1):71–90, 2009.

[14] A. A. Golubov, M. Yu. Kupriyanov, and E. Ilichev. The current-phase relation in josephson junctions. *Reviews of modern physics*, 76(2):411, 2004.

[15] A. Buzdin. Direct coupling between magnetism and superconducting current in the josephson φ 0 junction. *Physical review letters*, 101(10):107005, 2008.

[16] F. Konschelle and A. Buzdin. Magnetic moment manipulation by a josephson current. *Physical Review Letters*, 102(1):017001, 2009.

[17] R. Gross, A. Marx, and F. Deppe. *Applied superconductivity: Josephson effect and superconducting electronics*. De Gruyter, 2016.

[18] W. C. Stewart. Current-voltage characteristics of josephson junctions. *Applied physics letters*, 12(8):277–280, 1968.

[19] D. E. McCumber. Effect of ac impedance on dc voltage-current characteristics of superconductor weak-link junctions. *Journal of Applied Physics*, 39(7):3113–3118, 1968.

[20] C. Guarcello and F. S. Bergeret. Cryogenic memory element based on an anomalous josephson junction. *Physical Review Applied*, 13(3):034012, 2020.

[21] F. Dettwiler, J. Fu, et al. Stretchable persistent spin helices in gaas quantum wells. *Physical Review X*, 7(3):031010, 2017.

[22] Yu. M. Shukrinov, I. R. Rahmonov, and K. Sengupta. Ferromagnetic resonance and magnetic precessions in φ 0 junctions. *Physical Review B*, 99(22):224513, 2019.

[23] S. A. Abdelmoneim, Yu. M. Shukrinov, K. V. Kulikov, H.ElSamman, and M. Nashaat. Locking of magnetization and josephson oscillations at ferromagnetic resonance in a φ_0 junction under external radiation. *Phys. Rev. B*, 106:014505, Jul 2022.

[24] Yu. M. Shukrinov, I. R. Rahmonov, A. Janalizadeh, and M.R. Kolahchi. Anomalous gilbert damping and duffing features of the superconductor-ferromagnet-superconductor φ 0 josephson junction. *Physical Review B*, 104(22):224511, 2021.